



Probabilistic flutter analysis of a long-span bridge in typhoon-prone regions considering climate change and structural deterioration

Xiaolei Chu ^a, Wei Cui ^{a,b,*}, Lin Zhao ^{a,b,c}, Shuyang Cao ^{a,b}, Yaojun Ge ^{a,b}

^a State Key Lab of Disaster Reduction in Civil Engineering, Tongji University, Shanghai, 200092, China

^b Key Laboratory of Transport Industry of Bridge Wind Resistance Technologies, Tongji University, Shanghai, 200092, China

^c State Key Laboratory of Mountain Bridge and Tunnel Engineering, Chongqing Jiaotong University, Chongqing, 400074, China

ARTICLE INFO

Keywords:

Long-span bridge
Probabilistic flutter analysis
Typhoon hazard
Climate change
Structural deterioration
Generalized density evolution equation

ABSTRACT

In this paper, a long-term probabilistic flutter analysis of long-span bridges, with consideration of the time-variant probability density function (PDF) of annual maximum wind speed caused by climate change and the deterioration effects of dynamic properties obtained by field monitoring data, is investigated. Estimated uncertainty, which occurs in probabilistic flutter analysis, is quantified by the generalized density evolution equation (GDEE). A suspension bridge, with the center span of 1650 m, is chosen as application example. Long-term deterioration and inter-seasonal varying characteristics of modal frequencies and damping ratios are discussed. An implicit formulation among radius to maximum winds R_{\max} , central pressure deficit Δp , latitude ψ and sea surface temperature SST is set up by training a two-layer feed-forward artificial neural network (ANN) with historical records, and then the full-track typhoon simulation is conducted based on Vickery's empirical model. Lastly, long-term probabilistic flutter analysis is conducted in conjunction with three prospective climate change scenarios, RCP2.6, RCP4.5 and RCP8.5, showing that the likelihood of annual flutter failure will increase greatly mainly due to higher annual maximum wind speed in a warming climate.

1. Introduction

Long-span bridges are vulnerable and susceptible to long-term environmental corrosion (Vu and Stewart, 2000), changing wind climate (Lee and Ellingwood, 2017) and fatigue damage accumulation (Kwon and Frangopol, 2010), etc., which makes the structural reliability time-variant. The challenges posed by aging structures (Frangopol et al., 1997) and tropical cyclone hazard (Lee and Ellingwood, 2017) have prompted many researches to address risk management problems. In current engineering practice of wind-resistance design, flutter instability is not allowed in bridge's service state. Flutter-resistance performance for long-span bridges is related with two factors, on-site wind climate (i.e., probability distribution of annual maximum wind speed) and structural resistant capacity (i.e., flutter critical wind speed). As for in-service bridges, evaluation of flutter-resistance performance is more important since on-site wind climate and structural resistant capacity are both time-variant (Lee and Ellingwood, 2017), bringing significant uncertainty to structural safety. However, related investigations are still scarce (Wang et al., 2020; Yuen and Kuok, 2010). As a result, long-term probabilistic flutter analysis considering deteriorations of structural properties and possible climate changes will provide a comprehensive

insight into long-term structural performances (Ellingwood and Lee, 2016a,b).

Lots of long-span bridges are established along coastal regions of China, which are often invaded by tropical cyclones. Tropical cyclone, one of the most devastating weather phenomena, has motivated several investigations attempting to forecast tropical cyclone hazards in the future (Mudd et al., 2014a,b; Xu et al., 2020). Several statistical models have been developed for tropical cyclone simulations in wind engineering by Georgiou (1986), Simiu and Scanlan (1996) and Vickery et al. (2000a,b). Recently, Vickery's empirical track model has been widely adopted (Snaiki and Wu, 2020; Cui and Caracoglia, 2019; Fang et al., 2021) to incorporate climate change effects on wind hazard analysis (Seo and Caracoglia, 2015; Cui and Caracoglia, 2016) and risk assessment (Pant and Cha, 2019; Snaiki et al., 2020) along US Atlantic coastal regions, where sea surface temperature (SST) is chosen to reflect potential effects of climate change. For example, Lee and Ellingwood (2017) adopted Vickery's model to infer the non-stationary intensities and frequencies of hurricanes under various climate warming scenarios for intergenerational decision model. Cui and Caracoglia (2016) also employed Vickery's model and future SST under various climate warming scenarios to analyze the hurricane wind speed and to

* Correspondence to: 207 Wind Engineering Building, Tongji University, 1239 Siping Road, Shanghai, 200092, China.
E-mail address: cuiwei@tongji.edu.cn (W. Cui).

discuss its effects on structural damage and intervention costs. In Cui and Caracoglia (2016), however, estimated uncertainty simultaneously occurred while fitting the long-term distribution parameters. Estimated uncertainty caused by fitting residuals was not considered and might bring with large bias. What is more, neither Lee and Ellingwood (2017) nor Cui and Caracoglia (2016) considered the effects of SST while estimating the wind speed at gradient height by Georgiou's gradient wind field model (Georgiou, 1986), in other words, SST was only considered in the track model.

For long-span bridges, modal frequencies and damping ratios are two important modal properties for flutter resistant capacity (Theodorsen, 1949). In existing studies, flutter analysis for long-span bridges has been conducted by several researchers through experiments or numerical simulations (Ji et al., 2020; Fang et al., 2020). However, investigations of flutter probability for in-service long-span bridges are extremely rare, especially considering the structural deterioration obtained by structural health monitoring (SHM) data (Wang et al., 2020; Xu and Xia, 2011). By SHM data, effects of structural deteriorations on long-term flutter analysis can be considered.

For probabilistic flutter analysis, several methods are developed. The first order reliability method (FORM) is widely used, for example, Ge et al. (2000) employed FORM to estimate flutter failure of Yangpu Bridge; Baldomir et al. (2013) adopted modified FORM to consider uncertainties in damping ratios, flutter derivatives and wind velocity for probabilistic flutter analysis. The sampling method, such as Monte-Carlo Simulation (MCS), is another estimation method with good accuracy. For example, Caracoglia (2013) utilized the Euler MCS to analyze randomness of bridge flutter speed, based on assessment of Moment Lyapunov exponent of system stability. Mannini and Bartoli (2015) approached probabilistic flutter analysis considering uncertainties in flutter derivatives and investigated the uncertainty propagation. Furthermore, Canor et al. (2015) compared the results of flutter probability by different stochastic methods (random perturbation, collocation method, Galerkin approach, MCS, etc.). Though the MCS is accurate, it suffers from low efficiencies especially for long-term flutter analysis with time-variant modal properties. It takes longer time for computations since a single change in modal properties will need a recalculation of corresponding flutter critical wind speed. Actually, in this paper, what we need in probabilistic flutter analysis is PDF of flutter critical wind speed. As a result, it will be more convenient if a relationship between the PDF of flutter critical wind speed and PDFs of structural properties can be established.

This paper proposes a generalized framework for probabilistic flutter analysis considering effects of climate change and structural deterioration, by using typhoon simulations and SHM data. This paper is organized as follows. Firstly, Vickery's full-track typhoon simulation method is reviewed, then is conducted on the Northwestern Pacific under three climate warming scenarios RCP2.6, RCP4.5 and RCP8.5 (Stocker et al. (2013) define Representative Concentration Pathways as RCP). A two-layer feed-forward artificial neural network (ANN) is trained by historical records from the International Best Track Archive for Climate Stewardship (IBTrACS) (Knapp et al., 2018), where SST is also imported to reflect the effects of climate change on Georgiou's gradient wind field model. Then, the non-stationary PDF of annual maximum wind speed in a warming climate is discussed. Secondly, one of the authors' previous work (Chu et al., 2021) is briefly introduced to illustrate the structural deterioration effects. Structural deterioration phenomenon of a suspension bridge in China is discussed, where modal frequencies and damping ratios are time-variant. By regression analysis of modal properties extracted from long-term SHM data, the deterioration rules and inter-seasonal varying characteristics of modal properties can be gained (Chu et al., 2021; Yuen and Kuok, 2010). A linear regression model is proposed to obtain the PDF of flutter critical wind speed if PDFs of modal properties are given, avoiding a repetitive sampling process. Thirdly, in order to quantify the estimated uncertainty that occurs in fitting the long-term distribution parameters

of annual maximum wind speeds, the generalized density evolution equation (GDEE) (Li and Chen, 2008, 2009) is employed. It shows that the warming climate and structural deteriorations will tremendously increase the likelihood of annual flutter failure, which should be considered in engineering practice. What is more, estimated uncertainty will bring with remarkable bias and is necessary for consideration.

2. Warming climate and synthetic typhoon simulations

2.1. Potential effects of increasing SST on tropical cyclone activity

Different Representative Concentration Pathways (RCPs) have been utilized to quantify different climate change effects (Stocker et al., 2013). Under RCP8.5 scenario, the increment of temperatures in Atlantic Ocean is about 4 °C, and only concentrates on a limited region (Cui and Caracoglia, 2016). However, the temperatures are expected to increase extensively at most 7 °C under RCP8.5 scenario in Northwestern Pacific, which will influence the tropical cyclone activities greatly. The projections of global mean temperature in August 2100 are illustrated in Fig. 1, based on the database from the Canadian Centre for Climate Modeling and Analysis (Flato et al., 2000).

SST is the power source of tropical cyclones. It has been validated that the frequency and intensity of tropical cyclones may vary as a result of fluctuating SST values (Emanuel, 1987). As for the intensity, it is believed that more intense tropical cyclones will occur in a warming climate, as concluded in Mudd et al. (2014a,b). On the other hand, the warmer SST appears to positively exacerbate the occurrence of tropical cyclones. By examining the historical hurricane database (HurDat) (Cui and Caracoglia, 2016), the mean annual frequency of hurricanes in the North Atlantic Ocean has been increasing indeed. However, as indicated in Webster et al. (2005), against a background of increasing SST, no global trend has yet emerged in the number of tropical cyclones in other regions. Many researchers studied the past variations of typhoon frequency in Northwestern Pacific (Lee et al., 2012a,b; Ma and Chen, 2009). Lee et al. (2012b) showed that there is a nominally positive trend in typhoon frequency and duration in the Joint Typhoon Warning Center (JTWC) data for 1945–2007, though they did not report on the statistical significance of the trends. Ma and Chen (2009) showed a decreasing tendency over time in the typhoon frequency for the basin (1949–2007). The historical trend of typhoon occurrence in Northwestern Pacific is plotted according to the results in the IBTrACS Project (Knapp et al., 2018) in Fig. 2(a), where the annual typhoon number is counted by all typhoons that occurred in Northwestern Pacific in each year. As shown in Fig. 2(a), it is obvious that generally, the observed typhoon number each year increased sharply in the period 1884–1970, then fell down in general since 1970s. The increasing trend in 1884–1970 might be related to several factors, such as the increasing SST and more advanced observing technologies. However, the observed typhoon numbers declined later, which presented an inverse regularity compared with the general trend in the North Atlantic Ocean (Cui and Caracoglia, 2016). Cui and Caracoglia (2016) also pointed that the trend of an increment of hurricane frequency is not guaranteed for Atlantic Ocean due to various reasons, and for some locations the hurricane frequency may also decrease.

As a result, the PDF of annual typhoon occurrence rate is temporarily regarded as time-invariant in this study, which is to be reconsidered when a more accurate estimating method appears. Conventionally, the arrival rate of rare hazards has been modeled by a Poisson process (Simiu and Scanlan, 1996; Mudd et al., 2014a; Li and Ellingwood, 2006). While, Vickery et al. (2000a) employed the Negative Binomial distribution. Both models are validated in Fig. 2(b). Kolmogorov-Smirnov test (Massey Jr, 1951) is performed to examine the fitting goodness. With 0.05 confidence level, the *p*-values are 0.6722 and 5.76×10^{-7} for Negative Binomial and Poisson distributions, respectively. The null hypothesis that Poisson model fits the distribution of the annual typhoon frequency is rejected. Hence, Negative Binomial distribution is employed here.

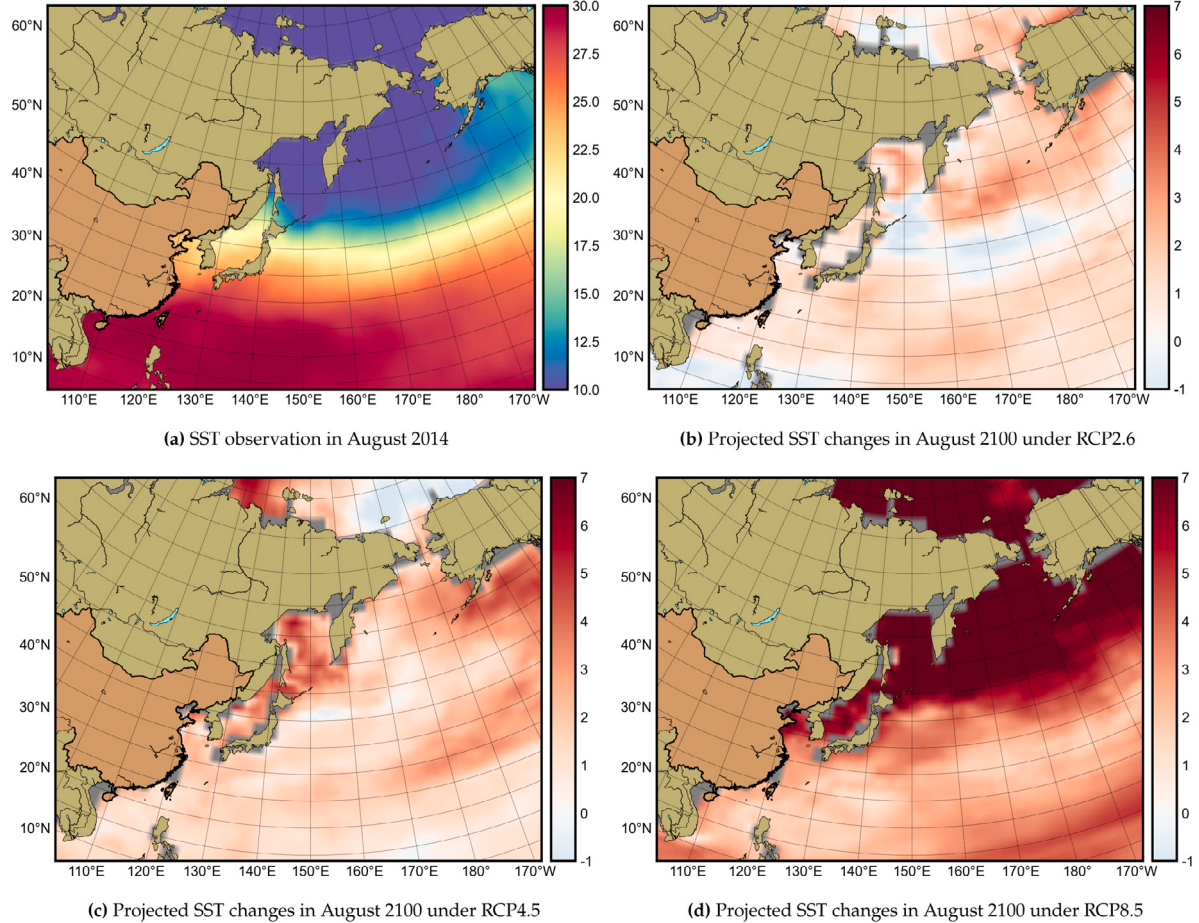


Fig. 1. Historical SST and projected SST changes under various climate warming scenarios - reproduced from the Canadian Centre for Climate Modeling and Analysis (Flato et al., 2000).

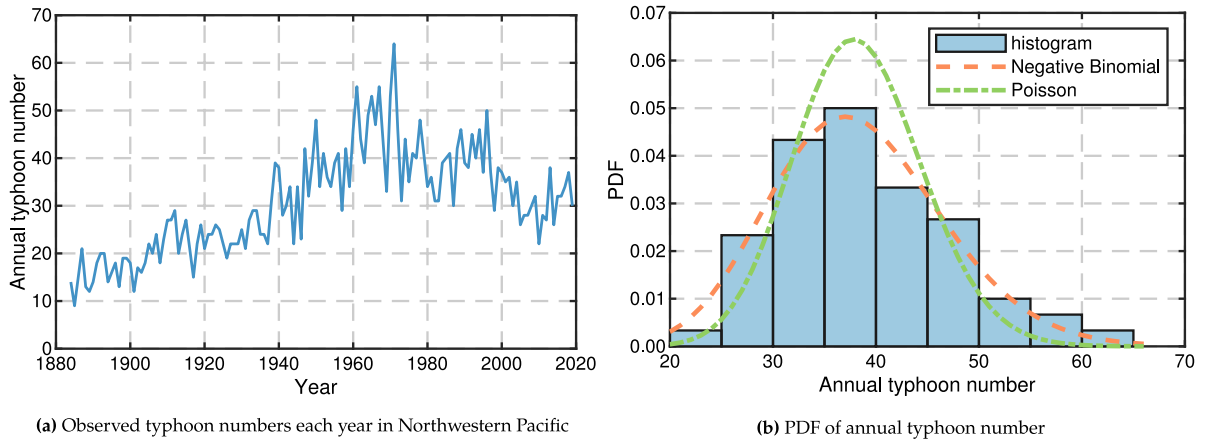


Fig. 2. Observed annual typhoon numbers and corresponding PDF.

2.2. Vickery's full-track simulation model

Quantification of the typhoon hazard is a necessary step to appropriately evaluate the wind speed at a specific place. Vickery's model (Vickery et al., 2000a,b) is a powerful tool for typhoon simulations, utilizing statistical properties of historical typhoon initiations, tracks and intensities (Knapp et al., 2018).

Vickery's track model (Vickery et al., 2000a) simulates the typhoon translation velocity, heading, and the relative intensity. These quantities are expressed in Eqs. (1), (2) and (3):

$$\Delta \ln c = a_1 + a_2 \psi + a_3 \lambda + a_4 \ln c_i + a_5 \theta_i + \epsilon_c \quad (1)$$

$$\Delta \theta = b_1 + b_2 \psi + b_3 \lambda + b_4 \ln b_i + b_5 \theta_i + b_6 \theta_{i-1} + \epsilon_\theta \quad (2)$$

$$\ln(I_{i+1}) = c_0 + c_1 \ln(I_i) + c_2 \ln(I_{i-1}) + c_3 \ln(I_{i-2}) + c_4 T_s + c_5 (\Delta T_s) + \epsilon_I \quad (3)$$

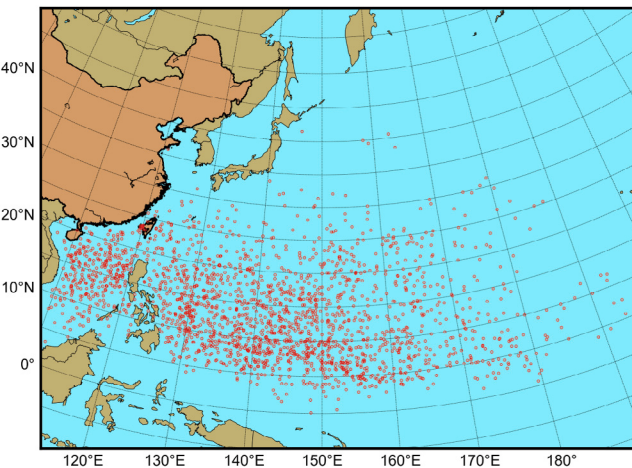


Fig. 3. Locations of typhoon genesis in Northwestern Pacific from IBTrACS database (Knapp et al., 2018).

where $a_i (i = 1, 2, \dots, 5)$ and $b_i (i = 1, 2, \dots, 6)$ are coefficients obtained by regression analysis from historical records; ψ and λ are latitude and longitude of the typhoon center, respectively; c_i is the typhoon translation speed at time step i ; θ_i is the typhoon heading at time step i , range of which is $-180^\circ \sim 180^\circ$, and $\theta = 0$ when the typhoon is heading north; the relative intensity I (Darling, 1991) is a dimensionless term, utilized to relate the actual typhoon pressure deficit Δp to the greatest possible central pressure deficit allowed by the average climatology of the typhoon season (Vickery et al., 2000a); T_s is the SST at time step $i + 1$, denoted as $\Delta T_s = T_{s_{i+1}} - T_{s_i}$; ϵ_c , ϵ_θ and ϵ_I are linear regression residuals.

Once a typhoon lands, energy accumulated from the sea is cut off, then the typhoon will decay. The intensity decay model (Vickery et al., 2000a) is

$$\Delta p(t) = \Delta p_0 \cdot \exp(-at_h) \quad (4)$$

$$a = a_0 + a_1 \Delta p + \epsilon_a \quad (5)$$

where $\Delta p(t)$ is the central pressure deficit; Δp_0 is the pressure deficit when the typhoon lands; a is the exponential decay rate over time t_h (in hours); a_0 and a_1 are site-specific parameters; ϵ_a is a linear regression residual.

It should be noted that the west-ward and east-ward typhoons are examined independently due to effects of Coriolis force (Cui and Caracoglia, 2016). The parameters in Eqs. (1)~(5) are obtained by QuadTree decomposition algorithm proposed by (Cui et al., 2020).

As for typhoon genesis (Vickery et al., 2000a; Cui and Caracoglia, 2019), the “birthplace” of typhoons are sampled randomly from IBTrACS database (Knapp et al., 2018). The initial “birthplace” in Northwestern Pacific is shown in Fig. 3.

2.3. Proposed R_{\max} formulation in Georgiou’s gradient wind field model trained by ANN

Gradient wind fields can be approximately modeled as a large vortex with a translation movement, where the gradient wind speed V_g can be decomposed into a rotational component V_R and a translation component V_T . The magnitude of V_R is a function that depends on the distance r from the typhoon center. As denoted in Georgiou (1986), V_g is determined by vector summation between V_R and V_T :

$$V_g = \frac{1}{2}(c \sin \alpha - fr) + \sqrt{\frac{1}{4}(c \sin \alpha - fr)^2 + \frac{100B\Delta p}{\rho} \left(\frac{R_{\max}}{r}\right)^B \exp \left[-\left(\frac{R_{\max}}{r}\right)^B\right]} \quad (6)$$

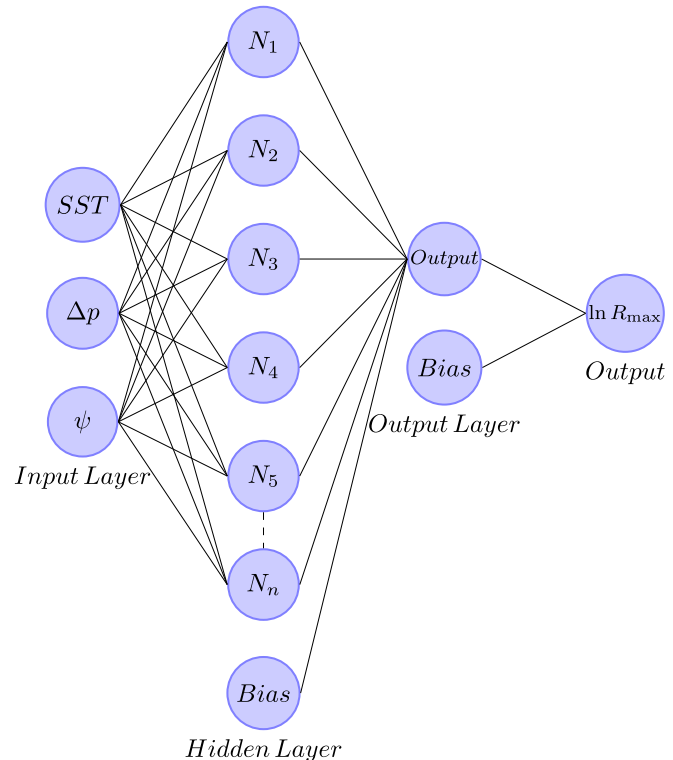


Fig. 4. Two-layer feed-forward neural network.

where c is the translation speed; α is the relative angle between the heading direction and radial position; R_{\max} is the radius to maximum winds; B is the Holland parameter.

Previous studies (Cui and Caracoglia, 2016; Lee and Ellingwood, 2017) adopted the original formulation introduced by Vickery et al. (2000a), where R_{\max} only depends on Δp and ψ and involves simple nonlinearity. The original formulation is

$$\ln R_{\max} = 2.636 - 0.00005086\Delta p^2 + 0.0394899\psi, \quad r^2 = 0.2765 \quad (7)$$

The original R_{\max} formulation is imperfect, where the fitting goodness is $r^2 = 0.2765$. In order to improve the fitting performance and introduce more nonlinear relations comprehensively, as presented in Fig. 4, an ANN model with sigmoid hidden neurons and linear output neurons is trained, using typhoon records in Northwestern Pacific. What is more, SST, along with ψ and Δp , is also adopted as an input. Hence, the variation of SST caused by different climate warming scenarios is taken into consideration in the wind field model.

By hyperparameter tuning, it is found that six hidden neurons are appropriate to minimize the mean squared error (i.e., largest r^2 values). Fig. 5 illustrates the three-element input-layer ANN results obtained using one hidden layer with six neurons: 70% of the data set is chosen for training, while 15% is set aside for validation and the rest for testing. As shown in Fig. 5, the x axis, “Target Values”, means the real R_{\max} value from historical records (Knapp et al., 2018) given Δp , ψ and SST; the y axis, “Output Values”, means the predicted R_{\max} value by the proposed ANN model. If the prediction is completely correct, the scattered points will distribute along the dashed line “ $r^2 = 1$ ”. Fig. 5 shows that the ANN model, with $r^2 \approx 0.44$, performs better than Eq. (7).

3. Synthetic typhoon generation considering climate change: results and discussions

3.1. Statistical comparisons at various Kilometer-Posts (KPs)

The validity of the proposed synthetic typhoon simulation methodology in Northwestern Pacific has been investigated in Cui et al. (2020).

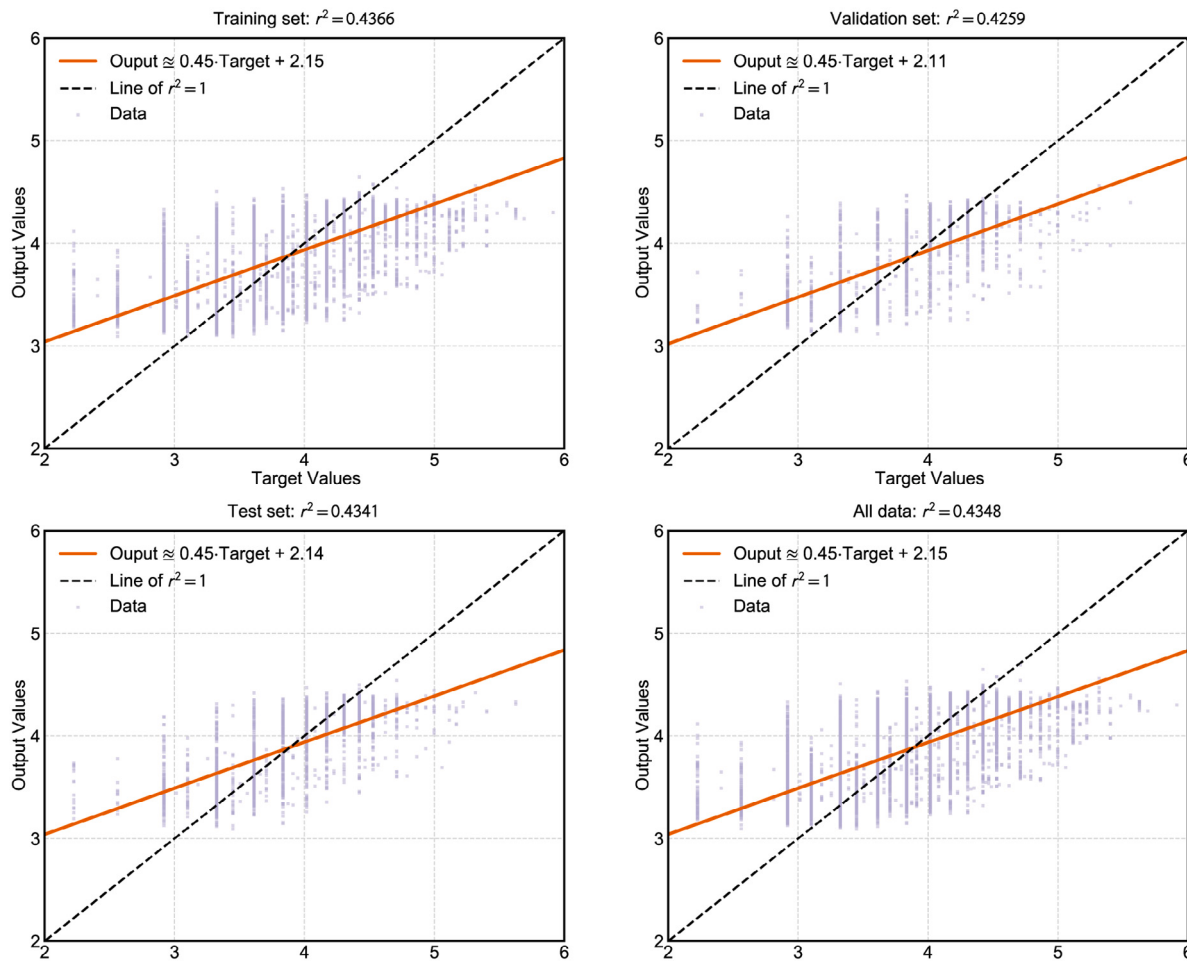


Fig. 5. Performance of the two-layer feed-forward neural network with sigmoid hidden neurons and linear output neurons (data sources used here are from IBTrACS ([Knapp et al., 2018](#))).

Usually, annual occurrence rate, translation speed, heading, and pressure deficit at predefined Kilometer-Posts (KPs) are four key factors of the typhoon simulation, which was proposed by [Georgiou \(1986\)](#) and widely used by researchers ([Snaiki and Wu, 2020](#); [Cui and Caracoglia, 2016](#)). In this paper, predefined KPs along Chinese coastline are shown in [Fig. 6](#), ranging from the border between China and Vietnam to the border between China and Korea. The distance between two adjacent KPs is 500 km.

[Fig. 7](#) compares four key factors along Chinese coastline with three different climate change scenarios. Historical SST in year 2010 is chosen as a baseline for comparison. RCP2.6, RCP4.5, and RCP8.5 are chosen as three representative climate warming scenarios to reflect climate change conditions. All SST values are obtained from the Canadian Centre for Climate Modeling and Analysis ([Flato et al., 2000](#)). For different SST condition in each year, the full-track typhoon simulation is conducted based on 100-year samplings, in order to get reliable statistical characteristics ([Cui et al., 2020](#)). For each climate warming scenario, therefore, there will be 9000-year samplings, where time ranges uniformly from year 2010 to year 2100 (90 “epochs” of 100-year duration, i.e., 9000 years in total).

For annual occurrence rate in [Fig. 7\(a\)](#), it generally remains unchanged under various climate warming conditions. This is because the PDF of typhoon genesis number is considered to be time-invariant, as explained in Section 2.1. However, the annual occurrence rates at KP 1~20 are relatively higher under climate warming scenarios. The reason is that though the typhoon genesis number remains the same under climate warming scenarios, yet increasing SST will prolong the duration of a typhoon process ([Emanuel, 1987](#)). This reason leads to

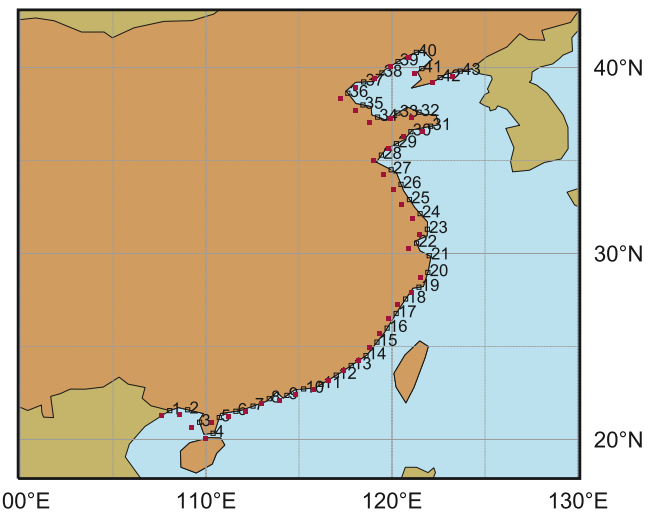


Fig. 6. Predefined Kilometer-Posts along Chinese coastline.

more typhoon landfalls, which would originally decayed in the Pacific ocean and would not land on coastal regions. As a result, higher occurrence rates are recorded at KP 1~20. What is more, based on Eq. (3), larger SST and less uniformly-distributed variations of SST contribute to a larger and slowly-varying intensities.

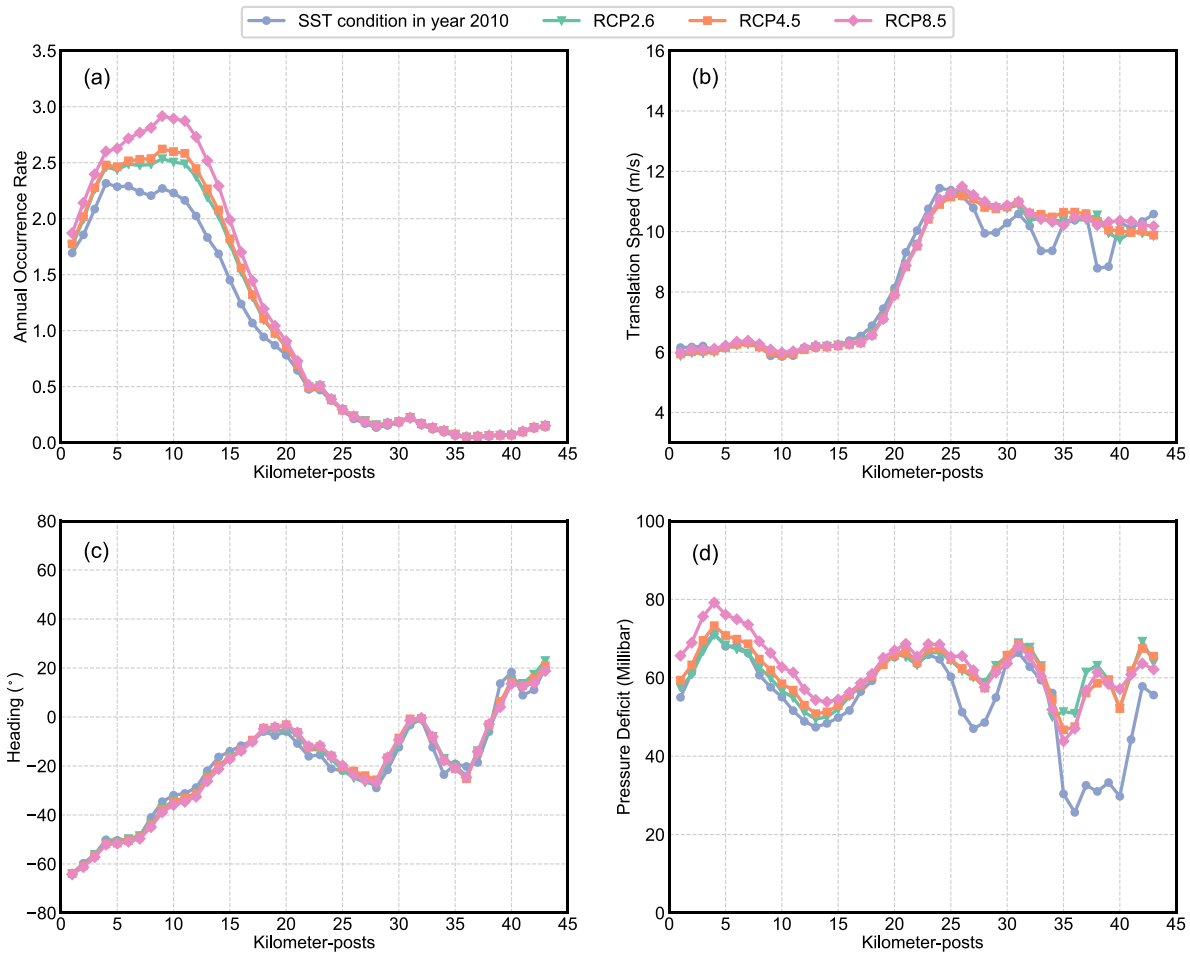


Fig. 7. Synthetic typhoon generation: a comparison among annual occurrence rate, translation speed, heading and pressure deficit under non climate change condition (SST condition in 2010 is chosen as baseline) and RCP2.6, RCP4.5, RCP8.5 climate warming scenarios.

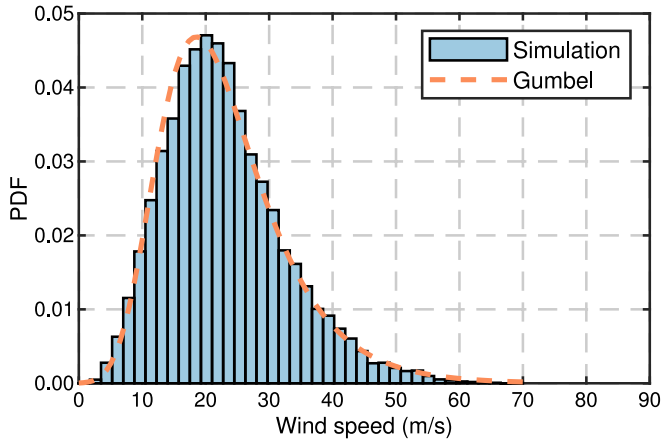


Fig. 8. Simulated annual gradient wind speed maximum distribution (m/s) at Zhoushan City.

For typhoon translation speed and heading, as shown in Figs. 7(b)–(c), the variation under different climate warming scenarios is negligible. The reason is that the translation speed Eq. (1) and the heading Eq. (2) do not involve SST, which are limitations of Vickery's model (Vickery et al., 2000a). As a result, different SST conditions will not make much difference.

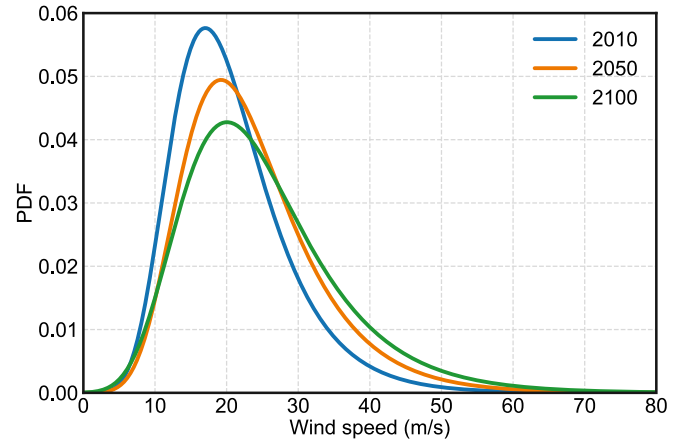


Fig. 9. Variation of the wind speed PDF with RCP8.5 scenario, in Shenzhen.

In Fig. 7(d), there are obvious increments of typhoon pressure deficit with climate warming scenarios, compared with those in year 2010. This means that typhoons are intensified by higher SST (Emanuel, 1987). The increments of typhoon pressure deficit are more remarkable in KP 35~43 due to more significant increments of SST in northern Pacific in Fig. 1(d). Since the variation of SST in Northwestern Pacific is not homogeneous, the variation of pressure deficit is also different

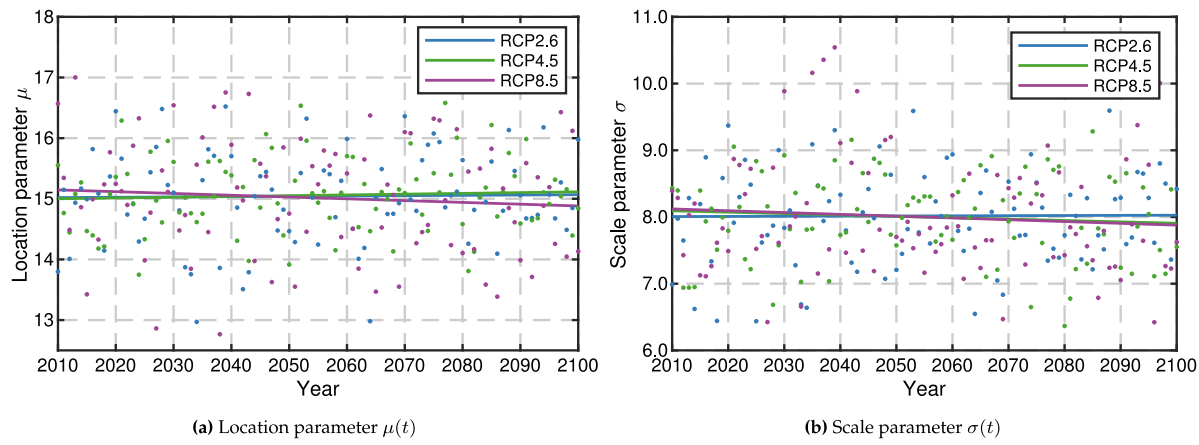
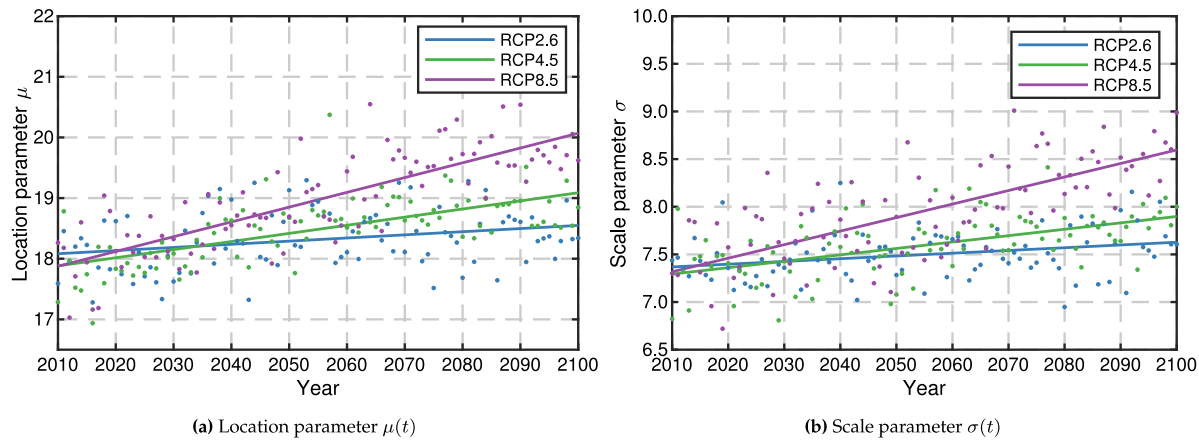
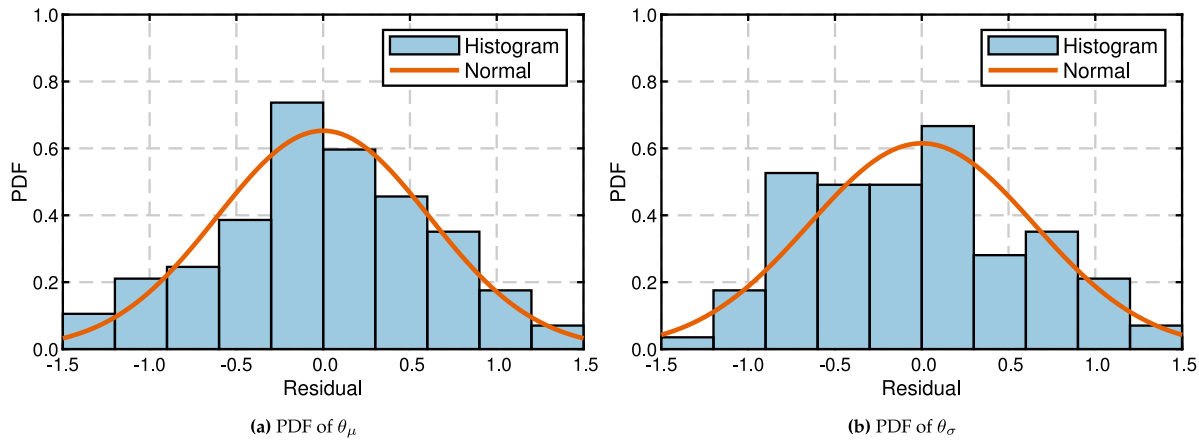
Fig. 10. Time-variant Gumbel distribution parameters $\mu(t)$ and $\sigma(t)$ in Zhoushan.Fig. 11. Time-variant Gumbel distribution parameters $\mu(t)$ and $\sigma(t)$ in Shenzhen.

Fig. 12. Normally-distributed fitting residuals of distribution parameters.

along KPs. What is more, the increments of typhoon pressure deficit (i.e., the typhoon intensity) are also locally-dependent. For example, around KP 33, the pressure deficit will slightly decrease in the warming climate.

3.2. Non-stationary distribution parameters of wind speed PDF in warming climates

Along with the full-track typhoon simulation and the ANN R_{\max} model, the PDF of annual maximum wind speed at a specific place

can be obtained. For example, the probability distribution of annual maximum wind speed at the gradient height in Zhoushan City ($30.06^\circ N, 121.92^\circ E$) is plotted in Fig. 8 for clarification, based on historical SST condition in year 2010. The Gumbel distribution (Chen et al., 2018) is employed to fit the empirical histogram of the gradient wind speed in Fig. 8, as described in Eq. (8).

$$f(v; \mu(t), \sigma(t)) = \left(\frac{1}{\sigma(t)} \right) \exp \left(-\exp \left(-\frac{v - \mu(t)}{\sigma(t)} \right) - \frac{v - \mu(t)}{\sigma(t)} \right) \quad (8)$$

where $\mu(t)$ is the location parameter and $\sigma(t)$ is the scale parameter; t is the time, unit of which is year. If the distribution parameters are non-stationary, $\mu(t)$ and $\sigma(t)$ will change with t (Cui and Caracoglia, 2016).

The Kolmogorov-Smirnov test (Massey Jr, 1951) is utilized to test the feasibility of Gumbel distribution. The test shows that Gumbel distribution fits well with $p = 0.4765$, which indicates that Gumbel distribution passes the test at a significance level 0.05. In this study, it is found that Gumbel distribution fits the probability distribution of annual maximum wind speed in coastal regions of China well. As a result, Gumbel distribution is adopted for annual maximum wind speed with climate change effects.

In the context of climate change, the PDF of annual maximum wind speed will change with time, which means $\mu(t)$ and $\sigma(t)$ in Eq. (8) are time-variant. For example, Fig. 9 presents the variation of the wind speed PDF in Shenzhen City ($22.59^\circ N, 113.96^\circ E$) with RCP8.5 scenario for year 2010, year 2050 and year 2100, respectively. To investigate the long-term variation, distribution parameters $\mu(t)$, $\sigma(t)$ of simulated results are fitted over time by linear regression.

Zhoushan City is located around KP 21. In Fig. 10, time-variant Gumbel distribution parameter $\mu(t)$ and $\sigma(t)$ are plotted. By linear regression, the long-term variation of $\mu(t)$ and $\sigma(t)$ will not change significantly. It is reasonable because in Fig. 7(d), the typhoon pressure deficit and annual landing rate around KP 21 does not change significantly under various climate warming scenarios, which means the typhoon around KP 21 is not intensified.

In Fig. 11, however, $\mu(t)$ and $\sigma(t)$ for Shenzhen City are increasing over time, and the non-stationary characteristics are remarkable. As shown in Fig. 6, Shenzhen City locates around KP 10. According to Fig. 7(d), at KP 10, the typhoon pressure deficit becomes larger with higher SST, which leads to more intensive typhoons and more larger wind speeds.

Meanwhile, Figs. 10 and 11 show that both $\mu(t)$ and $\sigma(t)$ are dispersedly distributed. The dispersion is caused by the significantly-fluctuating SST condition in each year, as indicated in Cui and Caracoglia (2016). Therefore, it is necessary to quantify the estimated uncertainty caused by fitting the long-term $\mu(t)$ and $\sigma(t)$.

As shown in Eq. (9), the non-stationary distribution parameters can be expressed by linear equations, combined with random variables caused by the fitting residuals. In this study, the Normal distribution is adopted to fit the residuals.

$$\mu(t; \theta_\mu) = a_\mu t + b_\mu + \theta_\mu \quad (9a)$$

$$\sigma(t; \theta_\sigma) = a_\sigma t + b_\sigma + \theta_\sigma \quad (9b)$$

where a_i and b_i ($i = \mu, \sigma$) are constants obtained by regression; θ_μ and θ_σ are normally-distributed random variables as shown in Fig. 12, which are PDFs of fitting residuals. Denote $\Theta = \Theta(\theta_\mu, \theta_\sigma)$ to represent the estimated uncertainty caused by fitting residuals.

4. Structural deterioration and corresponding inter-seasonal varying characteristics

In this section, one of the authors' previous work (Chu et al., 2021) is briefly presented here to illustrate the structural deterioration phenomena and corresponding inter-seasonal varying characteristics.

4.1. Bridge description

As shown in Fig. 13, Xihoumen Bridge is a suspension bridge with a 1650-meter central main span located at Zhoushan City, linking Jintang Island and Cezi Island. The wind-resistance design for Xihoumen Bridge is important due to the challenging local wind climate (Zhao et al., 2019) and flexible structural properties.

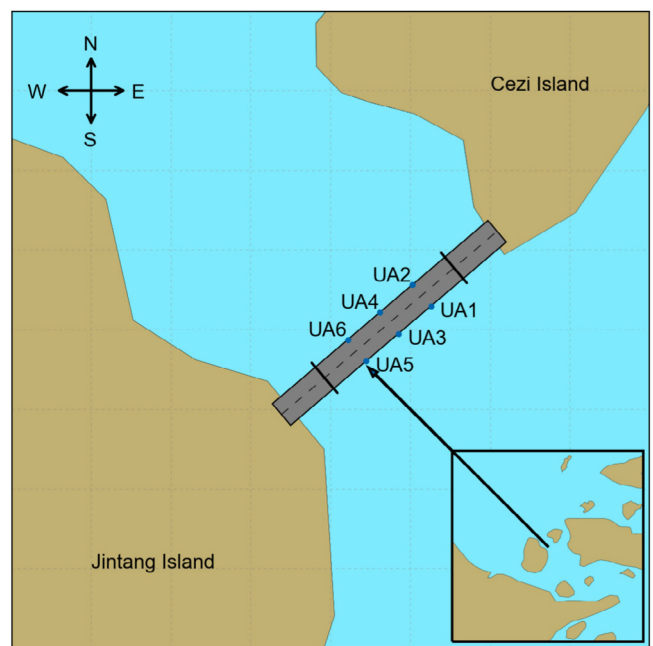


Fig. 13. Location of Xihoumen Bridge.

4.2. Modal frequencies

The time-variant deterioration functions of 1st-order vertical and torsional modal frequencies (Chu et al., 2021), fitted in Fig. 14, are based on historical data (from year 2010 to year 2015) of the Xihoumen SHM system. It is apparent that the modal frequencies are decreasing generally with bridge's aging due to various factors, such as material fatigues. The long-term deteriorations are defined by functions " f_{v1} " and " f_{t1} " (denoted by red lines in Fig. 14), where the unit of "t" is month.

Additionally, modal frequencies are fluctuating periodically around the long-term deterioration functions. The inter-seasonal varying characteristics might be caused by periodic temperature variations, periodic humidity variations, etc. (Ni et al., 2005; Xia et al., 2006), which are modeled as random variables ϵ_{v1} , ϵ_{t1} in Fig. 14 (Chu et al., 2021). The PDFs of inter-seasonal varying characteristics (i.e., ϵ_{v1} and ϵ_{t1}) are shown in Fig. 15.

4.3. Damping ratios

Corresponding damping ratios are presented in Fig. 16. Compared with modal frequencies, the long-term deterioration phenomenon of damping ratios is ambiguous, however, the variability, i.e., the inter-seasonal characteristics, is much more remarkable. As a result, the long-term deteriorations of damping ratios are ignored, and only inter-seasonal varying characteristics are considered, i.e., the damping ratios are modeled as random variables with constant PDFs as shown in Fig. 17.

5. Linear regression model for flutter critical wind speed and its probability density function

The flutter critical wind speed can be determined by the multi-mode approach and full-mode approach (Ge and Tanaka, 2000), with known modal frequencies, damping ratios and flutter derivatives. Ge and Tanaka (2000) elaborated the difference with various number of natural modes participating in the flutter by multi-mode flutter analysis, showing that the error between two modes (fundamental vertical mode and torsional mode) and multiple modes (up to 7 modes

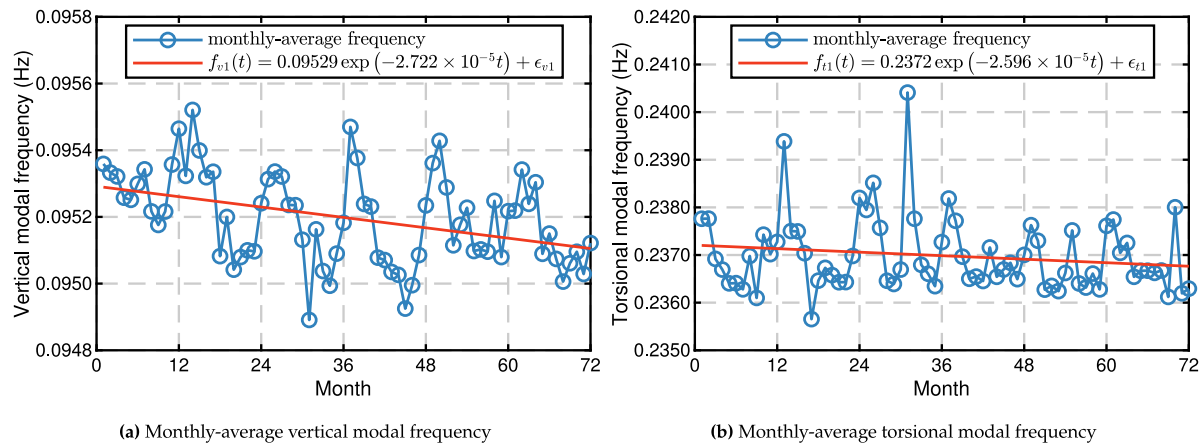


Fig. 14. Long-term deteriorations and corresponding inter-seasonal varying characteristics of modal frequencies.

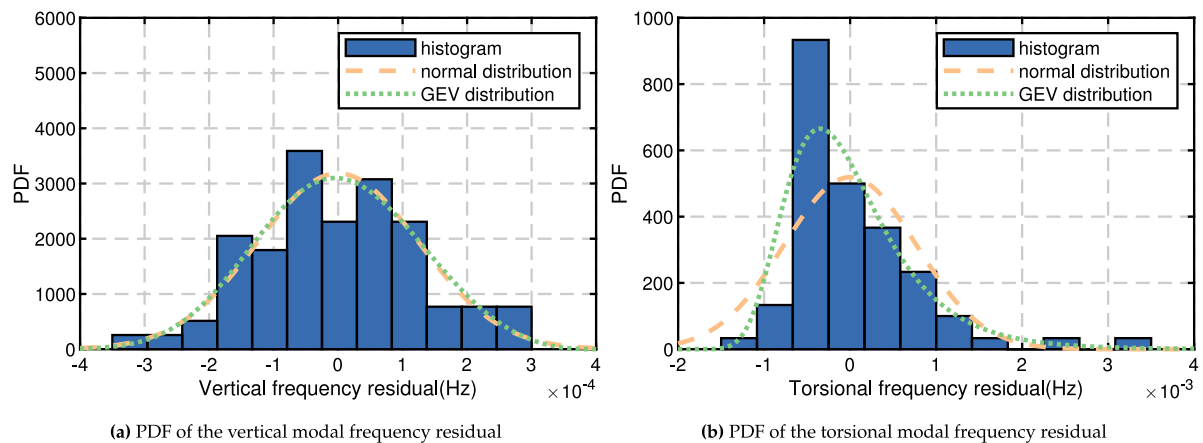


Fig. 15. Probability distributions of inter-seasonal varying characteristics.

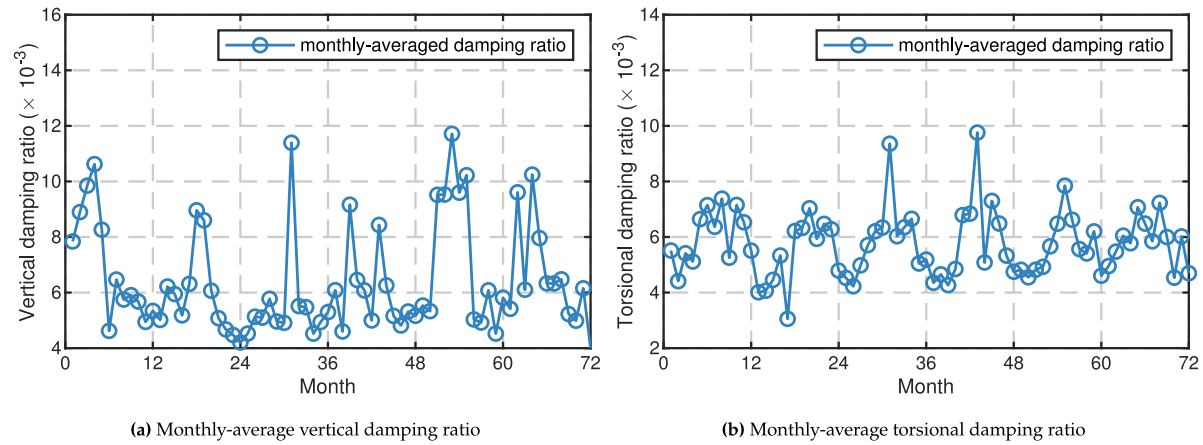


Fig. 16. Long-term deteriorations and corresponding inter-seasonal varying characteristics of damping ratios.

included) is less than 0.3%. As a result, only 1st-order vertical mode and 1st-order torsional mode are considered in this study, for Xihoumen Bridge.

For probabilistic flutter analysis, the accurate estimation for PDF of flutter critical wind speed is usually conducted by Monte-Carlo Simulation (Seo and Caracoglia, 2011), involving a time-consuming sampling process of uncertain modal properties. It will be more efficient if we could obtain the PDF of flutter critical wind speed once given PDFs of modal properties. As a result, a linear regression model (Eq. (10)) is

proposed here to avoid a repetitive sampling process.

$$V_R = \alpha_{v1} f_{v1} + \alpha_{t1} f_{t1} + \beta_{v1} \zeta_{v1} + \beta_{t1} \zeta_{t1} + c \quad (10)$$

where α_{v1} , α_{t1} , β_{v1} , β_{t1} and c are regression coefficients; f_{v1} , ζ_{v1} and f_{t1} , ζ_{t1} are modal frequencies and damping ratios, respectively for 1st-order vertical mode and 1st-order torsional mode; V_R is the flutter critical wind speed. In Eq. (10), the variance of V_R is completely determined by variances of f_i and ζ_i ($i = v1, t1$). In other words, if the PDFs of f_i and ζ_i are given, the PDF of V_R is deterministic. For the same modal mode,

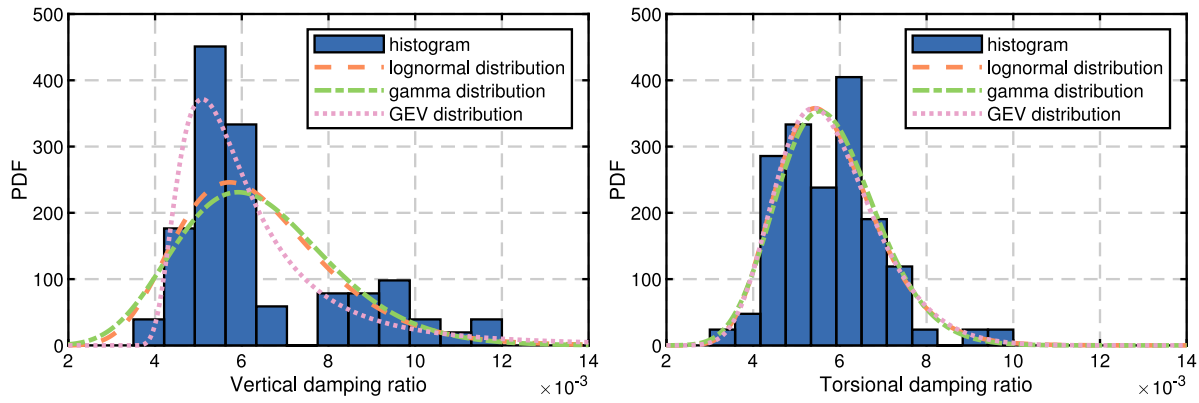


Fig. 17. PDFs of vertical and torsional damping ratios.

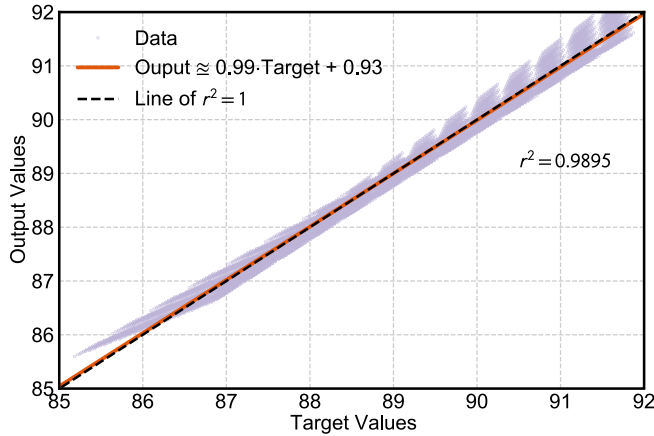


Fig. 18. Fitting goodness of the proposed linear regression model.

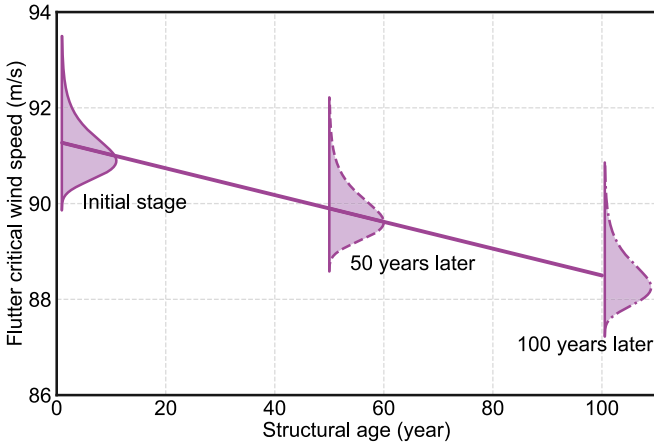
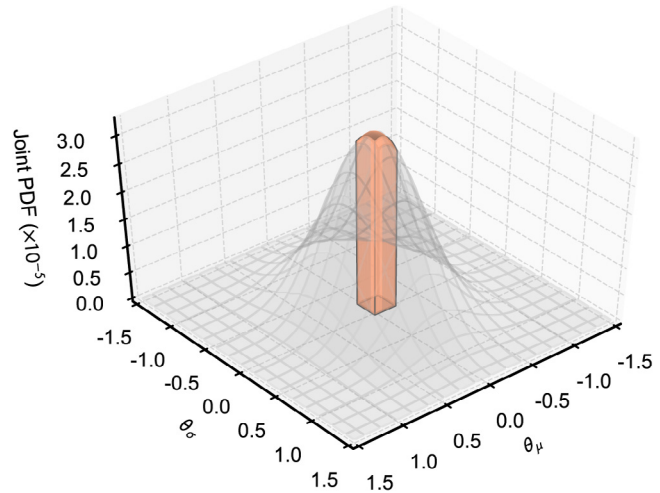


Fig. 19. Evolving PDF of the flutter critical wind speed with bridge's aging.

the variance of f_i is independent with the variance of ζ_i based on SHM results (Chu et al., 2021). Then, the PDF of V_R can be derived (Petrov, 2012) as below:

$$f_R(r) = \frac{1}{|\alpha_{v1}\alpha_{t1}\beta_{v1}\beta_{t1}|} \iiint_{-\infty}^{+\infty} f_{f,v1}\left(\frac{x_1}{\alpha_{v1}}\right) f_{f,t1}\left(\frac{x_2 - x_1}{\alpha_{t1}}\right) \\ \times f_{\zeta,v1}\left(\frac{x_3 - x_2}{\beta_{v1}}\right) f_{\zeta,t1}\left(\frac{r - x_3 - c}{\beta_{t1}}\right) dx_1 dx_2 dx_3 \quad (11)$$

Fig. 20. Random parameter space Ω_Θ and representative volume V_q . (For interpretation of the references to color in this figure legend, the reader is referred to the web version of this article.)

where $f_{f,i}(\cdot)$ ($i = v1, t1$) denote PDFs of modal frequencies; $f_{\zeta,i}(\cdot)$ ($i = v1, t1$) denote PDFs of damping ratios; $f_R(r)$ denotes the corresponding PDF when flutter critical wind speed equals to r .

In order to include the entire possible life-cycle structural properties, ranges of f_{v1} , f_{t1} , ζ_{v1} and ζ_{t1} are set as $(0.090, 0.100)$, $(0.226, 0.238)$, $(0.004, 0.012)$ and $(0.003, 0.010)$, respectively. Each set is divided linearly with 100 parts, and the flutter critical wind speed is calculated by multi-mode approach (Ge and Tanaka, 2000) at each selected point, given the flutter derivatives in Chu et al. (2021). In Fig. 18, “Target values” are the specific theoretical flutter critical wind speeds by multi-mode approach (Ge and Tanaka, 2000) when given a specific set of modal frequencies and damping ratios; “Output values” are the calculated flutter critical wind speeds by Eq. (10) when given the same specific set of modal frequencies and damping ratios. The regression result is presented in Fig. 18, where $r^2 = 0.9895$, showing a good fitting performance. Notably, Eq. (10) is only valid in the specific parameter range predefined in this study and not necessarily correct in the whole parameter range. What is more, Eq. (10) and Fig. 18 are bridge-specific, which are applicable for Xihoumen Bridge but not definitely right for other bridges.

Choose the modal frequencies and damping ratios in June each year as the representative modal properties in that year. With bridge's aging, the evolving PDF of flutter critical wind speed due to structural deteriorations can be obtained by Eq. (11) in Fig. 19 (Chu et al., 2021).

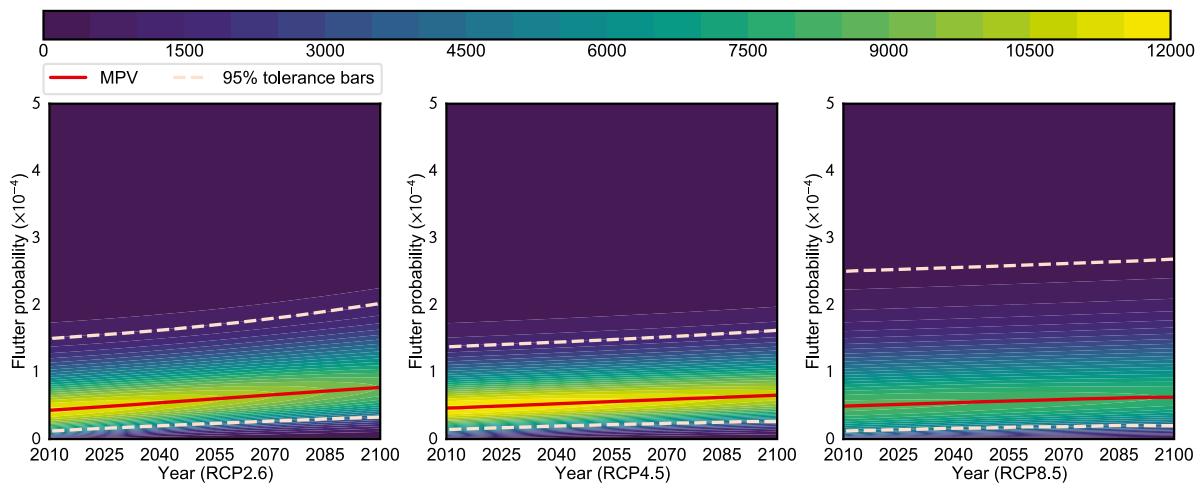


Fig. 21. Evolution process with RCP2.6, RCP4.5, and RCP8.5 climate change scenarios, combined with the wind speed distribution in Zhoushan City. (For interpretation of the references to color in this figure legend, the reader is referred to the web version of this article.)

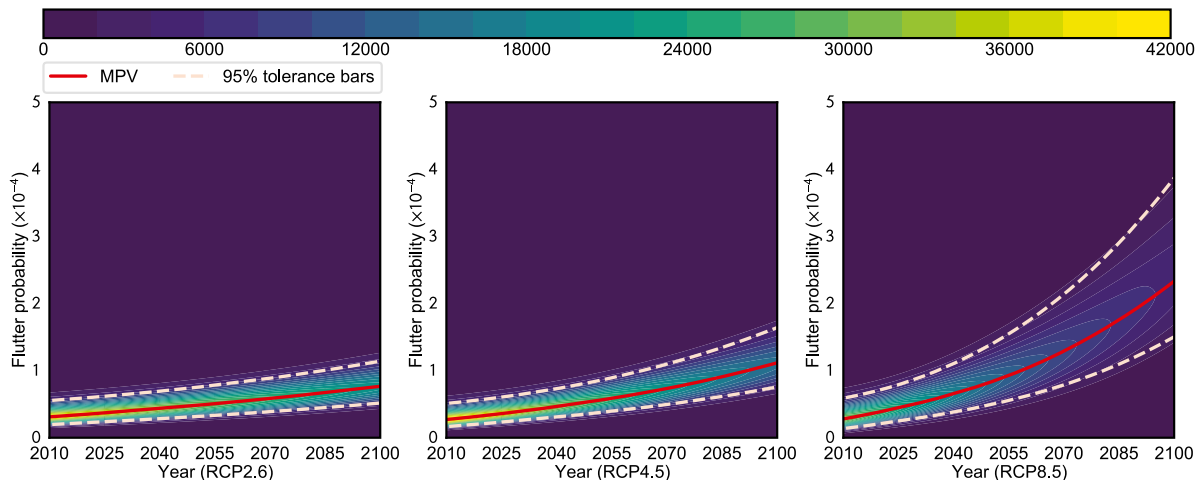


Fig. 22. Evolution process with RCP2.6, RCP4.5, and RCP8.5 climate change scenarios, combined with the wind speed distribution in Shenzhen City.

6. Methodology to assess flutter probability and quantify estimated uncertainty

In this study, the determination of flutter probability is a typical structural reliability problem (Melchers and Beck, 2018), involving only one load effect S (i.e., annual maximum wind speed) and one resistance R (i.e., flutter critical wind speed). The determination of flutter probability is easy if each is described by a known and deterministic PDF, $f_S(s)$ and $f_R(r)$ respectively. However, due to the existence of estimated uncertainty Θ , $f_S(s)$ is not deterministic. In this section, the generalized density evolution equation is introduced to quantify this estimated uncertainty.

6.1. Methodology

Denote $V_S(t)$ is the wind speed at a certain place, obeying a time-variant PDF $f_S(s, t)$; $V_R(t)$ is the flutter critical wind speed, also obeying a time-variant PDF $f_R(r, t)$. Then, a state function $Z(t)$ can be defined as below.

$$Z(t) = V_R(t) - V_S(t) \quad (12)$$

Flutter occurs when $Z(t) < 0$. The flutter probability is $E[Z(t) < 0]$, where $E[\cdot]$ is the mathematical expectation. Due to the estimated uncertainty Θ in Eq. (9), $f_S(s, t)$ is not deterministic even if the time

t is given, which will lead to uncertainty for determination of flutter probability. Utilize $f_S(s, t, \Theta)$ to denote $f_S(s, t)$ with estimated uncertainty Θ . Then the flutter probability (Melchers and Beck, 2018) is a stochastic process

$$F(t, \Theta) = E[Z(t, \Theta) < 0] = \iint_{r \leq s} f_R(r, t) \cdot f_S(s, t, \Theta) dr ds \quad (13)$$

where $F(t, \Theta)$ denotes the flutter probability at time t , with randomness caused by estimated uncertainty Θ .

When viewing from the random event description of the principle of preservations of probability (Li and Chen, 2009), it can be found that the randomness involved in $F(t, \Theta)$ completely originates from estimated uncertainty Θ , which can be solve by the generalized density evolution equation.

From Li and Chen (2008, 2009), if the joint PDF of $(F(t, \Theta), \Theta)$ is denoted by $p_{F\Theta}(f, \theta, t)$, it follows that

$$\frac{D}{Dt} \int_{D_f \times D_\Theta} p_{F\Theta}(f, \theta, t) df d\theta = 0 \quad (14)$$

where $\Theta = \Theta(\theta_\mu, \theta_\alpha)$, and the domains of Θ are presented in Fig. 20.

Noting the arbitrariness of $D_f \times D_\Theta$, we have (Li and Chen, 2009)

$$\frac{\partial p_{F\Theta}(f, \theta, t)}{\partial t} + \dot{F}(\theta, t) \frac{\partial p_{F\Theta}(f, \theta, t)}{\partial f} = 0 \quad (15a)$$

$$\dot{F}(\theta, t) = \frac{df F(\theta, t)}{dt} \quad (15b)$$

The marginal probability distribution of $p_{F\Theta}(f, \theta, t)$ can then be given by

$$p_F(f, t) = \int_{\Omega_\Theta} p_{F\Theta}(f, \theta, t) d\theta \quad (16)$$

where Ω_Θ is the distribution domain of Θ , and $p_F(f, t)$ is the PDF of flutter probability when time = t and flutter probability $F = f$.

6.2. Computational procedure for generalized density evolution equation (GDEE)

The computational procedure for GDEE is explained in this section.

Firstly, select representative points in the random parameter space Ω_Θ . Denote the point set as $\mathcal{P} = \{\theta_q = (\theta_{1,q}, \theta_{2,q}, \dots, \theta_{s,q}) : q = 1, 2, \dots, n_{sel}\}$, where s is the number of the entire random variables involved, and n_{sel} is the cardinal number of the point set. In this paper, $s = 2$ (because Θ only contains two random variables, θ_μ and θ_σ in Eq. (9)) and $n_{sel} = 20$, which is accurate enough as verified in Appendix. It should be noted that $n_{sel} = 20$ is problem-specific and not definitely right in other cases. For each representative point θ_q , a representative domain V_q exists (Conway and Sloane, 2013), marked as the colored volume in Fig. 20.

$$P_q = \int_{V_q} p_\Theta(\theta) d\theta \quad (17)$$

Surely, $\sum_{q=1}^{n_{sel}} P_q = 1$. The initial conditions (Li and Chen, 2009) are partially discretized correspondingly to

$$p_{F\Theta}(f, \theta_q, t_0) = p_{F_0}(f) P_q \quad (18)$$

where $q = 1, 2, \dots, n_{sel}$.

Secondly, for each θ_q , implement deterministic analysis when setting $\Theta = \theta_q$, then get the velocity of $\dot{F}(\theta_q, t)$.

Thirdly, for each θ_q , introduce $\dot{F}(\theta_q, t)$ into the following discretized version:

$$\frac{\partial p_{F\Theta}(f, \theta_q, t)}{\partial t} + \dot{F}(\theta_q, t) \frac{\partial p_{F\Theta}(f, \theta_q, t)}{\partial f} = 0 \quad (19)$$

where $q = 1, 2, \dots, n_{sel}$.

Solve this equation under the initial conditions with the finite difference method. In this step, the space (f, t) should be meshed. Denote the nodes of the mesh by (f_i, t_k) , $i = 0, 1, 2, \dots, k = 0, 1, \dots$, where $f_i = i\Delta f$, $t_k = k\Delta t$. Then Eq. (19) can be solved to obtain the values of the density at the nodes, denoted by $p_{F\Theta}(f_i, \theta_q, t_k)$.

Lastly, synthesize the results to get the instantaneous density through the discretized version:

$$p_F(f_i, t_k) = \sum_{q=1}^{n_{sel}} p_{F\Theta}(f_i, \theta_q, t_k) \quad (20)$$

In this paper, the GDEE is numerically solved with one-sided difference schemes, and the numerical stability is guaranteed when $0 \leq \dot{F}(\theta_q, t) \times \frac{\Delta t}{\Delta f} \leq 1$ (Li and Chen, 2009). The results calculated by GDEE are validated by Monte-Carlo Simulation (MCS) in Appendix.

6.3. Results and discussions

6.3.1. Case i: effects of climate change are weak

Xihoumen Bridge is located at Zhoushan City. As explained in Section 3.2, the long-term effect of climate change in Zhoushan City is not remarkable. As a result, the long-term variation of flutter probability is mainly caused by structural deteriorations. The long-term variation of flutter probability under various climate warming scenarios are presented in Fig. 21. The colorbar means the PDF of flutter probability, i.e., p_F in Eq. (16). All three evolution processes show a similar regularity: the mean value of flutter probability keeps on increasing with time.

Denote MPV to stand for the most probable value, which means the flutter probability with maximum p_F . In Fig. 21, the red line means MPV. The pink dashed lines means the 95% tolerance bars. According to the MPV, structural deteriorations will approximately increase the annual flutter failure probability from 5×10^{-5} to 8×10^{-5} . However, there is remarkable uncertainty while estimating the real annual flutter failure probability since the 95% tolerance area is large.

6.3.2. Case ii: effects of climate change are remarkable

In order to further investigate the potential impacts of climate change, the non-stationary distribution parameters $\mu(t)$, $\sigma(t)$ in Shenzhen City under various RCP scenarios are applied to Xihoumen Bridge, then the evolution process considering climate change and structural deteriorations simultaneously can be obtained, as presented in Fig. 22. Compared with that in Zhoushan City, the variation of the flutter failure probability caused by climate change is more remarkable, and the uncertainty becomes much more dispersed in the later stage of the evolution process.

The MPV of annual flutter failure probability in Shenzhen City will approximately increase from 3×10^{-5} to at most 24×10^{-5} with RCP8.5 scenario. The uncertainty for estimation of annual flutter failure probability is relatively smaller than that in Zhoushan City.

7. Conclusion

This paper proposes a methodology for long-term probabilistic flutter analysis of long-span bridges, considering the potential effects of climate change and structural deteriorations. Firstly, this study conducts the full-track typhoon simulation with various climate warming scenarios, based on Vickery's model. An implicit R_{max} formulation is established to incorporate effects of SST on Georgiou's wind field model for the first time. The possible non-stationary distribution parameters are discussed, and corresponding long-term variations are modeled as stochastic processes, where estimated uncertainty caused by fitting residuals are considered. Secondly, one of the authors' previous work is introduced to clarify the structural deterioration and inter-seasonal varying characteristics of dynamic properties, i.e., modal frequencies and damping ratios. Then a linear regression model between flutter critical wind speed and structural properties is established, which is able to directly obtain the PDF of flutter critical wind speed if given PDFs of structural properties, and also avoids a repetitive sampling process. Thirdly, effects of estimated uncertainty are discussed by generalized density evolution equation, indicating that the fiercely-fluctuating distribution parameters will bring with large errors when estimating annual flutter failure probability. Lastly by an application example, it shows that in Chinese typhoon-prone regions, simultaneous effects of climate change and structural deteriorations will increase the annual flutter failure probability from 3×10^{-5} to at most 24×10^{-5} . This study shows that structural deteriorations and climate change, which are usually neglected for the flutter analysis, should be considered for designs of long-span bridges.

CRediT authorship contribution statement

Xiaolei Chu: Writing - original draft, Conceptualization, Validation, Visualization. **Wei Cui:** Supervision, Writing - review & editing, Conceptualization, Visualization. **Lin Zhao:** Funding acquisition. **Shuyang Cao:** Project administration. **Yaojun Ge:** Supervision, Funding acquisition.

Declaration of competing interest

The authors declare that they have no known competing financial interests or personal relationships that could have appeared to influence the work reported in this paper.

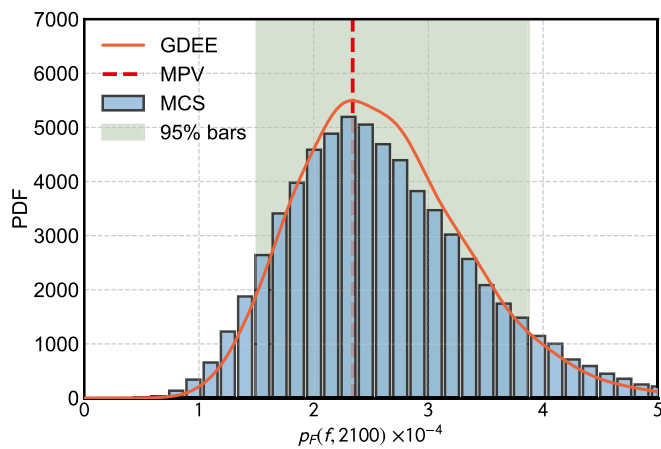


Fig. A.23. Comparison between GDEE and MCS with RCP8.5 scenario in year 2100, in Shenzhen.

Acknowledgments

The authors gratefully acknowledge the support of National Natural Science Foundation of China (52008314, 51778495, 51978527, 51678451), Shanghai Pujiang Program, China (No. 19PJ1409800), and National Key research and Development Program of China (2018YFC0809600). Any opinions, findings and conclusions are those of the authors and do not necessarily reflect the reviews of the above agencies.

Appendix. Comparison between GDEE and MCS

In order to validate the results by GDEE in Section 6.3, Monte-Carlo simulation (MCS) is employed. In Fig. A.23, located in Shenzhen City, the flutter probability with RCP8.5 scenario in year 2100 is shown. As presented, the result by GDEE has a good consistence with that by MCS.

References

- Baldomir, A., Kusano, I., Hernandez, S., Jurado, J., 2013. A reliability study for the Messina Bridge with respect to flutter phenomena considering uncertainties in experimental and numerical data. *Comput. Struct.* 128, 91–100.
- Canor, T., Caracoglia, L., Denoël, V., 2015. Application of random eigenvalue analysis to assess bridge flutter probability. *J. Wind Eng. Ind. Aerodyn.* 140, 79–86.
- Caracoglia, L., 2013. An Euler-Monte Carlo algorithm assessing moment Lyapunov exponents for stochastic bridge flutter predictions. *Comput. Struct.* 122, 65–77.
- Chen, A., Ma, R., Wang, D., Liu, G., Ai, H., Liu, T., 2018. Wind-resistant Design Specification for Highway Bridges. Ministry of Communications of the People's Republic of China, Beijing, China, (in Chinese).
- Chu, X., Sinh, H.N., Cui, W., Zhao, L., Ge, Y., 2021. Life-cycle assessment for flutter probability of a long-span suspension bridge based on field monitoring data.
- Conway, J.H., Sloane, N.J.A., 2013. Sphere Packings, Lattices and Groups, vol. 290. Springer Science & Business Media.
- Cui, W., Caracoglia, L., 2016. Exploring hurricane wind speed along US atlantic coast in warming climate and effects on predictions of structural damage and intervention costs. *Eng. Struct.* 122, 209–225.
- Cui, W., Caracoglia, L., 2019. A new stochastic formulation for synthetic hurricane simulation over the north Atlantic ocean. *Eng. Struct.* 199, 109597.
- Cui, W., Zhao, L., Cao, S., Ge, Y., 2020. Bayesian Optimization of typhoon full-track simulation on the Northwestern Pacific segmented by QuadTree decomposition. *J. Wind Eng. Ind. Aerodyn.* 104428.
- Darling, R., 1991. Estimating probabilities of hurricane wind speeds using a large-scale empirical model. *J. Clim.* 4 (10), 1035–1046.
- Ellingwood, B.R., Lee, J.Y., 2016a. Life cycle performance goals for civil infrastructure: intergenerational risk-informed decisions. *Struct. Infrastructure Eng.* 12 (7), 822–829.
- Ellingwood, B.R., Lee, J.Y., 2016b. Managing risks to civil infrastructure due to natural hazards: communicating long-term risks due to climate change. In: Risk Anal. Nat. Hazards. Springer, pp. 97–112.
- Emanuel, K.A., 1987. The dependence of hurricane intensity on climate. *Nature* 326 (6112), 483–485.
- Fang, G., Cao, J., Yang, Y., Zhao, L., Cao, S., Ge, Y., 2020. Experimental uncertainty quantification of flutter derivatives for a PK section girder and its application on probabilistic flutter analysis. *J. Bridge Eng.* 25 (7), 04020034.
- Fang, G., Pang, W., Zhao, L., Rawal, P., Cao, S., Ge, Y., 2021. Toward a refined estimation of typhoon wind hazards: Parametric modeling and upstream terrain effects. *J. Wind Eng. Ind. Aerodyn.* (ISSN: 0167-6105) 209, 104460.
- Flato, G., Boer, G., Lee, W., McFarlane, N., Ramsden, D., Reader, M., Weaver, A., 2000. The Canadian centre for climate modelling and analysis global coupled model and its climate. *Clim. Dynam.* 16 (6), 451–467.
- Frangopol, D.M., Lin, K.-Y., Estes, A.C., 1997. Life-cycle cost design of deteriorating structures. *J. Struct. Eng.* 123 (10), 1390–1401.
- Ge, Y., Tanaka, H., 2000. Aerodynamic flutter analysis of cable-supported bridges by multi-mode and full-mode approaches. *J. Wind Eng. Ind. Aerodyn.* 86 (2–3), 123–153.
- Ge, Y., Xiang, H., Tanaka, H., 2000. Application of a reliability analysis model to bridge flutter under extreme winds. *J. Wind Eng. Ind. Aerodyn.* 86 (2–3), 155–167.
- Georgiou, P.N., 1986. Design wind speeds in tropical cyclone-prone regions.
- Ji, X., Huang, G., Zhao, Y.-G., 2020. Probabilistic flutter analysis of bridge considering aerodynamic and structural parameter uncertainties. *J. Wind Eng. Ind. Aerodyn.* 201, 104168.
- Knapp, K.R., Diamond, H.J., Kossin, J.P., Kruk, M.C., Schreck, C.J., 2018. International best track archive for climate stewardship (ibtracs) project, version 4. <http://dx.doi.org/10.25921/82TY-9E16>, <https://data.noaa.gov/cgi-bin/iso?id=gov.noaa.ncdc:C01552>, type: dataset.
- Kwon, K., Frangopol, D.M., 2010. Bridge fatigue reliability assessment using probability density functions of equivalent stress range based on field monitoring data. *Int. J. Fatigue* 32 (8), 1221–1232.
- Lee, J.Y., Ellingwood, B.R., 2017. A decision model for intergenerational life-cycle risk assessment of civil infrastructure exposed to hurricanes under climate change. *Reliab. Eng. Syst. Saf.* 159, 100–107.
- Lee, T.-C., Knutson, T.R., Kamahori, H., Ying, M., 2012a. Impacts of climate change on tropical cyclones in the western North Pacific basin. Part i: Past observations. *Trop. Cyclone Res. Rev.* 1 (2), 213–235.
- Lee, T.-c., Leung, C.Y.-y., Kok, M.-h., Chan, H.-s., 2012b. The long term variations of tropical cyclone activity in the South China sea and the vicinity of Hong Kong. *Trop. Cyclone Res. Rev.* 1 (3), 277–292.
- Li, J., Chen, J., 2008. The principle of preservation of probability and the generalized density evolution equation. *Struct. Saf.* 30 (1), 65–77.
- Li, J., Chen, J., 2009. Stochastic Dynamics of Structures. John Wiley & Sons.
- Li, Y., Ellingwood, B.R., 2006. Hurricane damage to residential construction in the US: Importance of uncertainty modeling in risk assessment. *Eng. Struct.* 28 (7), 1009–1018.
- Ma, L.-P., Chen, L.-S., 2009. The relationship between global warming and the variation in tropical cyclone frequency over the western North Pacific. *J. Trop. Meteorol.* 15 (1), 38–44.
- Mannini, C., Bartoli, G., 2015. Aerodynamic uncertainty propagation in bridge flutter analysis. *Struct. Saf.* 52, 29–39.
- Massey Jr, F.J., 1951. The Kolmogorov-Smirnov test for goodness of fit. *J. Amer. Statist. Assoc.* 46 (253), 68–78.
- Melchers, R.E., Beck, A.T., 2018. Structural Reliability Analysis and Prediction. John Wiley & Sons.
- Mudd, L., Wang, Y., Letchford, C., Rosowsky, D., 2014a. Assessing climate change impact on the US east coast hurricane hazard: temperature, frequency, and track. *Nat. Hazards Rev.* 15 (3), 04014001.
- Mudd, L., Wang, Y., Letchford, C., Rosowsky, D., 2014b. Hurricane wind hazard assessment for a rapidly warming climate scenario. *J. Wind Eng. Ind. Aerodyn.* 133, 242–249.
- Ni, Y., Hua, X., Fan, K., Ko, J., 2005. Correlating modal properties with temperature using long-term monitoring data and support vector machine technique. *Eng. Struct.* 27 (12), 1762–1773.
- Pant, S., Cha, E.J., 2019. Potential changes in hurricane risk profile across the United States coastal regions under climate change scenarios. *Struct. Saf.* 80, 56–65.
- Petrov, V.V., 2012. Sums of Independent Random Variables, vol. 82. Springer Science & Business Media.
- Seo, D.-W., Caracoglia, L., 2011. Estimation of torsional-flutter probability in flexible bridges considering randomness in flutter derivatives. *Eng. Struct.* 33 (8), 2284–2296.
- Seo, D.-W., Caracoglia, L., 2015. Exploring the impact of “climate change” on lifetime replacement costs for long-span bridges prone to torsional flutter. *J. Wind Eng. Ind. Aerodyn.* 140, 1–9.
- Simiu, E., Scanlan, R.H., 1996. Wind Effects on Structures: Fundamentals and Applications to Design. John Wiley, New York.
- Snaiki, R., Wu, T., 2020. Revisiting hurricane track model for wind risk assessment. *Struct. Saf.* 87, 102003.
- Snaiki, R., Wu, T., Whittaker, A.S., Atkinson, J.F., 2020. Hurricane wind and storm surge effects on coastal bridges under a changing climate. *Transp. Res. Rec.* 0361198120917671.

- Stocker, T.F., Qin, D., Plattner, G.-K., Tignor, M., Allen, S.K., Boschung, J., Nauels, A., Xia, Y., Bex, V., Midgley, P.M., et al., 2013. Climate change 2013: The physical science basis. In: Contribution of Working Group I To the Fifth Assessment Report of the Intergovernmental Panel on Climate Change, vol. 1535.
- Theodorsen, T., 1949. General theory of aerodynamic instability and the mechanism of flutter.
- Vickery, P.J., Skerlj, P., Steckley, A., Twisdale, L., 2000b. Hurricane wind field model for use in hurricane simulations. *J. Struct. Eng.* 126 (10), 1203–1221.
- Vickery, P., Skerlj, P., Twisdale, L., 2000a. Simulation of hurricane risk in the US using empirical track model. *J. Struct. Eng.* 126 (10), 1222–1237.
- Vu, K.A.T., Stewart, M.G., 2000. Structural reliability of concrete bridges including improved chloride-induced corrosion models. *Struct. Saf.* 22 (4), 313–333.
- Wang, Y., Ni, Y., Zhang, Q., Zhang, C., 2020. Bayesian Approaches for evaluating wind-resistant performance of long-span bridges using structural health monitoring data. *Struct. Control Health Monit.* e2699.
- Webster, P.J., Holland, G.J., Curry, J.A., Chang, H.-R., 2005. Changes in tropical cyclone number, duration, and intensity in a warming environment. *Science* 309 (5742), 1844–1846.
- Xia, Y., Hao, H., Zanardo, G., Deeks, A., 2006. Long term vibration monitoring of an RC slab: temperature and humidity effect. *Eng. Struct.* 28 (3), 441–452.
- Xu, H., Lin, N., Huang, M., Lou, W., 2020. Design tropical cyclone wind speed when considering climate change. *J. Struct. Eng.* 146 (5), 04020063.
- Xu, Y.L., Xia, Y., 2011. Structural Health Monitoring of Long-Span Suspension Bridges. CRC Press.
- Yuen, K.-V., Kuok, S.-C., 2010. Ambient interference in long-term monitoring of buildings. *Eng. Struct.* 32 (8), 2379–2386.
- Zhao, L., Cui, W., Ge, Y., 2019. Measurement, modeling and simulation of wind turbulence in typhoon outer region. *J. Wind Eng. Ind. Aerodyn.* 195, 104021.